PERGAMON

International Journal of Solids and Structures 40 (2003) 1853–1864

INTERNATIONAL JOURNAL OF SOLIDS and STRUCTURES

www.elsevier.com/locate/ijsolstr

Analysis of shear band instabilities in compaction of powders

Pia Redanz *, Viggo Tvergaard

Department of Mechanical Engineering, Solid Mechanics, Technical University of Denmark, 2800 Kongens Lyngby, Denmark

Received 26 July 2002; received in revised form 18 November 2002

Abstract

A model for metal powder compaction is proposed as an interpolation between well-known models corresponding to a high level of porosity with low inter-particle cohesive strength or a low level of porosity with high cohesion. A simple model for analysis of shear band development in uniformly strained solids is used to study the possibility of flow localization during metal powder compaction. It is found that the material model predicts localization when the porosity is high and the cohesion is low, and localization is also predicted at intermediate levels of porosity, but not at low porosity levels where full cohesion applies.

Keywords: Shear band; Powder compaction; Porosity

1. Introduction

As a production process for obtaining near net final shape of complex-shaped engineering components, with good mechanical properties of the material, metal powder compaction and subsequent sintering has increasing importance. In the first part of the process, powder compaction, the success of the die compaction depends on obtaining defect-free green parts of approximately uniform density, and here modelling is an important tool. A micro-mechanically based material model has been developed by Fleck et al. (1992), relevant to high porosities in the early stage of compaction. These authors also suggested a combination of their FKM model with the Gurson model (1977) , more relevant to low porosities in the final stage, in order to cover the full range of porosities during a compaction process. Redanz (1999, 2001) has used these material models to analyse the powder compaction of a cup, comparing different compaction routes and ejection routes, and has shown that a wide variety of stress states may occur in the green part during the process.

If localization of plastic flow occurs during the powder compaction, this will tend to result in either a defect or in strongly non-uniform density. The possibility of shear band formation has been investigated by Redanz and Tvergaard (1999) based on the material model combining the FKM and Gurson models. This study focussed on shear localization under tensile loading in sintered metals, where the possibility of a

* Corresponding author.
E-mail address: pia@mek.dtu.dk (P. Redanz).

0020-7683/02/$ - see front matter © 2002 Elsevier Science Ltd. All rights reserved.
doi:10.1016/S0020-7683(03)00034-9

rather high level of porosity is relevant for real sintered components, but the study has also shown that no shear localization is predicted for compressive loading, even though it is well known that such instabilities occur in pressure sensitive materials like soils, which can only carry compressive stresses (e.g. see Rudnicki and Rice, 1975; Oda and Kazama, 1998). Soil-like behaviour is better accounted in the modified version of the FKM model proposed by Fleck (1995), where a cohesion factor was introduced, such that full inter-particle cohesion as well as no cohesion and intermediate cases can be represented. When the cohesion factor is close to zero the resulting yield surface resembles yield surfaces for cohesionless soils, consisting of a cone and a cap (e.g. Lade, 1977) or the Cam-Clay model of Schofield and Wroth (1968). Based on the material model of Fleck (1995) it has been shown by Tvergaard and Redanz (2001) that a cohesionless metal powder is prone to localization in shear bands during compaction.

In the present paper a combination of two porous material models is proposed, analogous to that proposed by Fleck et al. (1992). However, here the low cohesion model of Fleck (1995) is combined with the Gurson model, and furthermore the cohesion factor is described as porosity dependent. Thus the model is able to describe the realistic situation that the inter-particle cohesion is very low at high porosities, with the cohesion increasing slowly as the porosity is reduced, finally transforming into the full cohesion represented by the Gurson model when the material is fully compacted. This material model is used here to analyse the possibility of localization in shear bands during the compaction of a metal powder.

2. Porous material model

Fleck et al. (1992) proposed an approximate yield criterion for a particulate aggregate based on earlier work of Ashby and co-workers (e.g. Helle et al., 1985; Arzt, 1982; Arzt et al., 1983). They assumed that the porous material consists of spherical equi-sized particles bonded by isolated necks and that the particles move compatibly with the macroscopic strain. Fleck (1995) extended this model to account for reduced inter-particle cohesion by introducing a cohesion factor, η, for which fully sticking contacts are represented when $\eta = 1$ and no cohesive strength is present when $\eta = 0$. Redanz (1999) modified Fleck's yield criterion slightly to the form

$$\Phi_\eta = \left(\frac{5}{18}\frac{\sigma_e}{p_y} + \frac{2}{3}\right)^2 + \left(\frac{\sqrt{5}}{9}\frac{\sigma_k^k}{p_y}\right)^2 + \frac{5}{9}(1-\eta)\left(1 + \frac{\sigma_k^k}{3p_y} - \frac{1}{3}\frac{\sigma_e}{p_y}\right) - 1 = 0 \tag{1}$$

with the current yield stress of the matrix material, σ_M, and the void volume fraction or porosity, f. The von Mises stress, $\sigma_e = \sqrt{3 s_{ij} s^{ij}/2}$, where $s^{ij} = \sigma^{ij} - G^{ij}\sigma_k^k/3$ is the deviatoric stress tensor, and the yield strength of the porous material under hydrostatic loading

$$p_y = 2.97(1-f)^2 \frac{\hat{f} - f}{\hat{f}}\sigma_M \tag{2}$$

where $\hat{f} = 0.36$ is the porosity at dense random packing. This formulation of the yield criterion reduces to the FKM model (Fleck et al., 1992) for fully sticking contacts, $\eta = 1$. At porosities below about 0.25, the contacts start to interact and the particles become less and less spherical in shape. Hence, the micro-mechanically based particle model is applicable at high porosities only.

When powders are compacted, the inter-particle contacts weld together and true metallurgical bonds are formed. This would suggest some increase of η during the process. We model this phenomenon by including a dependency of η on the porosity, f, in the following form:

$$\eta = \begin{cases} \eta_a, & \text{for } f > f_a \\ \dfrac{(f-f_b)}{(f_a-f_b)}\eta_a + \dfrac{(f_a-f)}{(f_a-f_b)}\eta_b & \text{for } f_a > f > f_b \\ \eta_b, & \text{for } f < f_b \end{cases} \tag{3}$$

where η_a and η_b are initial and final cohesion factors, respectively. Hence, at porosities higher than f_a, the yield surface, Eq. (1), is used with $\eta = \eta_a$, at porosities lower than f_b, the cohesion factor is $\eta = \eta_b$, and for porosities in the range in between a linear interpolation of η_a and η_b is used.

At low porosities the porosity exists in form of isolated voids. Here, the micro-mechanical basis for the Gurson model (1977) is suitable. The appropriate yield condition is then

$$\Phi_{\mathrm{G}} = \frac{\sigma_e^2}{\sigma_{\mathrm{M}}^2} + 2q_1 f \cosh\left\{\frac{q_2}{2}\frac{\sigma_k^k}{\sigma_{\mathrm{M}}}\right\} - (1 + (q_1 f)^2) = 0 \tag{4}$$

where the constants $q_1 = 1.5$ and $q_2 = 1.0$ are included in order to bring the predictions of the model into closer agreement with full numerical analyses for periodic arrays of voids (see Tvergaard, 1981, 1982a).

In the present work, a combination of the two material models is used. At high porosities, $f > f_1$, the model (1) for low inter-particle cohesion is used and at low porosities, $f < f_2$, the Gurson model is used. In the transition range, $f_1 > f > f_2$, a linear combination of the material models is used, analogous to an interpolation used in Fleck et al. (1992), which results in the yield criterion

$$\Phi_{\mathrm{comb}} = w_\eta \Phi_\eta + w_{\mathrm{G}} \Phi_{\mathrm{G}} = 0 \tag{5}$$

where the weight functions are given by $w_\eta = (f - f_2)/(f_1 - f_2)$ and $w_{\mathrm{G}} = (f_1 - f)/(f_1 - f_2)$. Yield surfaces of different porosities are shown in Fig. 1.

It should be noted, that the Gurson model exhibits equal strength in tension and compression corresponding to full cohesion, $\eta = 1$, in the particle model. Hence, when the two models are combined, (5), the cohesion factor in Φ_η is increased in the range $\eta_a < \eta < \eta_b$ between f_a and f_b. But simultaneously the weight of Φ_η in (5) is reduced as f decays from f_1 to f_2, so that full cohesion is represented for $f < f_2$.

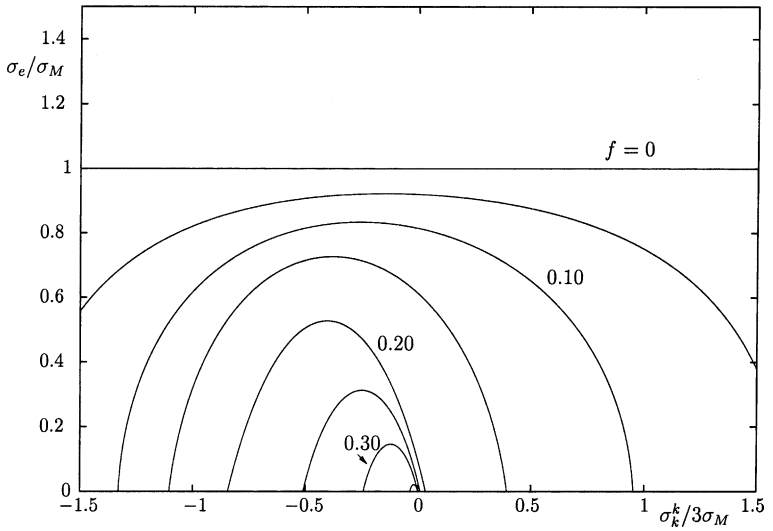

Fig. 1. Yield surface dependence on the hydrostatic pressure. Data in the material model, Eq. (5), are: $\eta_a = 0.001$, $\eta_b = 0.1$, $f_a = 0.30$, $f_b = 0.05$, $f_1 = 0.20$, and $f_2 = 0.01$.

The analysis is based on a convected co-ordinate Lagrangian formulation of the field equations in which the Lagrangian strain tensor is expressed by

$$\eta_{ij} = \tfrac{1}{2}(G_{ij} - g_{ij}) \tag{6}$$

where g_{ij} and G_{ij} are the metric tensors in the reference and current configuration, respectively. The total strain increment is taken to be the sum of the elastic and plastic parts

$$\dot{\eta}_{ij} = \dot{\eta}^{\mathrm{E}}_{ij} + \dot{\eta}^{\mathrm{P}}_{ij} \tag{7}$$

The material behaviour of the matrix is taken to be elastic-plastic with the uniaxial true stress-logarithmic strain relation given by the piecewise power law

$$\epsilon = \begin{cases} \sigma/E, & \text{for } \sigma \leqslant \sigma_{\mathrm{y}} \\ \dfrac{\sigma_{\mathrm{y}}}{E}\left(\dfrac{\sigma}{\sigma_{\mathrm{y}}}\right)^{n} & \text{for } \sigma > \sigma_{\mathrm{y}} \end{cases} \tag{8}$$

where E is Young's modulus, σ_{y} is the uniaxial yield stress, and n is the hardening exponent of the matrix material. Using the uniaxial stress–strain curve for the matrix material

$$\dot{\epsilon}^{\mathrm{P}}_{\mathrm{M}} = (1/E_t - 1/E)\dot{\sigma}_{\mathrm{M}} \tag{9}$$

and assuming that the macroscopic plastic work equals the microscopic plastic work, the following evolution equation for the tensile equivalent yield stress in the matrix material is obtained

$$\dot{\sigma}_{\mathrm{M}} = \frac{EE_t}{E - E_t}\frac{\sigma^{ij}\dot{\eta}^{\mathrm{P}}_{ij}}{F(f)\sigma_{\mathrm{M}}} \tag{10}$$

Here, E_t is the slope of the uniaxial stress–strain curve for the matrix material, and $F(f)$ represents the volume fraction of deforming material, which is different for the two yield criteria, (1) and (4), used here (see e.g. Fleck et al., 1992).

The change in porosity may be written as

$$\dot{f} = (1 - f)G^{ij}\dot{\eta}^{\mathrm{P}}_{ij} \tag{11}$$

when the contribution from the elastic part of the strain to the total change in volume is vanishing compared to the plastic contribution.

Macroscopic normality for the porous aggregate is assumed. Thus, the consistency condition, $\dot{\Phi} = 0$, leads to the plastic strain increment in the form

$$\dot{\eta}^{\mathrm{P}}_{ij} = \frac{1}{H}\frac{\partial \Phi}{\partial \sigma^{ij}}\frac{\partial \Phi}{\partial \sigma^{kl}}\overset{\nabla}{\sigma}{}^{kl} \tag{12}$$

with

$$H = -\left(\frac{\partial \Phi}{\partial f}(1 - f)G^{ij} + \frac{\partial \Phi}{\partial \sigma_{\mathrm{M}}}\frac{EE_t}{E - E_t}\frac{\sigma^{ij}}{F(f)\sigma_{\mathrm{M}}}\right)\frac{\partial \Phi}{\partial \sigma^{ij}} \tag{13}$$

where $(\overset{\nabla}{})$ denotes the Jaumann derivative. The constitutive relations are then obtained by using the elastic relationship

$$\overset{\nabla}{\sigma}{}^{ij} = \mathscr{R}^{ijkl}\dot{\eta}^{\mathrm{E}}_{kl} \tag{14}$$

(see e.g. Tvergaard, 1990).

3. Shear band model

The model used to predict the onset of localization in a homogeneously strained solid is illustrated in Fig. 2. A material inhomogeneity is present in a thin slice of material, which is assumed to be parallel with the x^3 axis and to have the initial orientation in the x^1–x^2 plane given by the initial angle of inclination, ψ_I, or the unit normal vector n_i. The initial porosity in the shear band is slightly higher, $f_I + \Delta f$, than the porosity in the material outside the band, f_I, hence, the value Δf represents the material inhomogeneity. The Cartesian coordinate system, x^{i}, is used as reference and the principal stress and strain directions outside the shear band are assumed to remain fixed and parallel to these axes throughout the deformation history. The stress states inside and outside the thin slice of material, respectively, are assumed to remain uniform. This type of model has been used earlier by a number of authors (Rice, 1976; Yamamoto, 1978; Tvergaard, 1981; Saje et al., 1982). An extension to also cover the post localization behaviour was used by Tvergaard (1982b).

The tangential derivatives of the displacement increments, $\dot{u}_i$, over the band interface have to be continuous due to compatibility. Thus, the derivatives of the displacement components inside the band are expressed by

$$\dot{u}^{\mathrm{b}}_{i,j} = \dot{u}^{\mathrm{o}}_{i,j} + \dot{c}_i n_j \tag{15}$$

in which $(\,)^{\mathrm{o}}$ and $(\,)^{\mathrm{b}}$ denote quantities outside and inside the band, respectively, and c_i are parameters to be determined. When no material inhomogeneity is present inside the band, the parameters c_i equal zero until bifurcation occurs. In the present study, the slightly higher porosity in the band leads to a softer material response inside the band than outside and hence the solution for c_i is non-trivial from the beginning. The onset of localization is then defined as the point where the material outside the band starts to unload. Equilibrium is expressed by

$$(\dot{T}^{\mathrm{i}})^{\mathrm{b}} = (\dot{T}^{\mathrm{i}})^{\mathrm{o}} \tag{16}$$

with the nominal tractions on the interface inside the band set equal to those outside the band. The nominal tractions on a surface with reference normal n_i are given by

$$T^{\mathrm{i}} = (\tau^{ij} + \tau^{kl} u^{\mathrm{i}}_{,k}) n_j \tag{17}$$

Different degrees of stress triaxiality are studied by using

$$\sigma^{\mathrm{o}}_2 = \kappa \sigma^{\mathrm{o}}_1 \tag{18}$$

where σ_i are the principal stresses and $\kappa = 0$ corresponds to uniaxial plane strain compression or uniaxial compression depending on the strain state

$$\epsilon^{\mathrm{o}}_3 = \gamma \epsilon^{\mathrm{o}}_2 \tag{19}$$

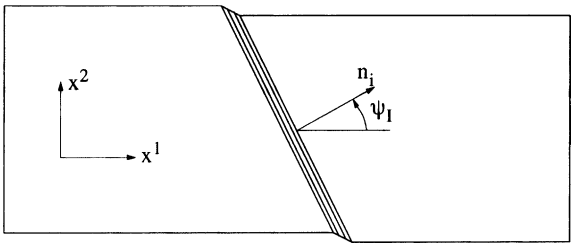

Fig. 2. Shear band model.

where ϵ_i are the principal logarithmic strains. Plane strain is obtained with $\gamma = 0$ and axisymmetric conditions outside the band with $\gamma = 1$.

The current angle of inclination, ψ, can be obtained from

$$\tan\psi = \exp(\epsilon_1^{\circ} - \epsilon_2^{\circ}) \tan\psi_I \tag{20}$$

at any stage of deformation.

4. Results

No shear band instabilities in compression occur in aggregates of powder with fully sticking inter-particle contacts, $\eta = 1$, or for other models representing full cohesion (see Redanz and Tvergaard, 1999). In contrast, stress states in compression leading to dilatation and thereby the possibility of shear band instabilities can occur for materials exhibiting low inter-particle strength, i.e. low values of η (see Tvergaard and Redanz, 2001). Hence, focus in the present work will be on rather high porosities, where the material model, Eq. (5) and Fig. 1, exhibits little cohesive strength. Data of the material to be analysed are $\sigma_y/E = 0.0033$, $\nu = 0.3$, and $n = 10$, and the parameters for the material model are set to $\eta_a = 0.001$, $\eta_b = 0.1$, $f_a = 0.30$, $f_b = 0.05$, $f_1 = 0.20$ and $f_2 = 0.01$. The resulting array of yield surfaces is shown in Fig. 1.

The imperfection sensitivity in a homogeneously strained solid is illustrated for different initial porosities in Fig. 3, where the logarithmic strain outside the band at localization, $-\epsilon_1^{\circ}$, vs. the initial porosity imperfection, Δf, is shown. Plane strain conditions, $\epsilon_3^{\circ} = 0$, are assumed, and the initial band orientation is set to $\psi_I = 55°$. The ratio between transverse and axial stresses is kept fixed at $\kappa = \sigma_2^{\circ}/\sigma_1^{\circ} = 0.10$. It is seen, that rather large porosity imperfections are necessary to trigger localization at lower initial porosities, f_I, i.e. when the material is more dense and the cohesive strength is no longer small. In each case, the critical strain is high at the lowest possible imperfection for localization to take place, but the critical strain is then re-

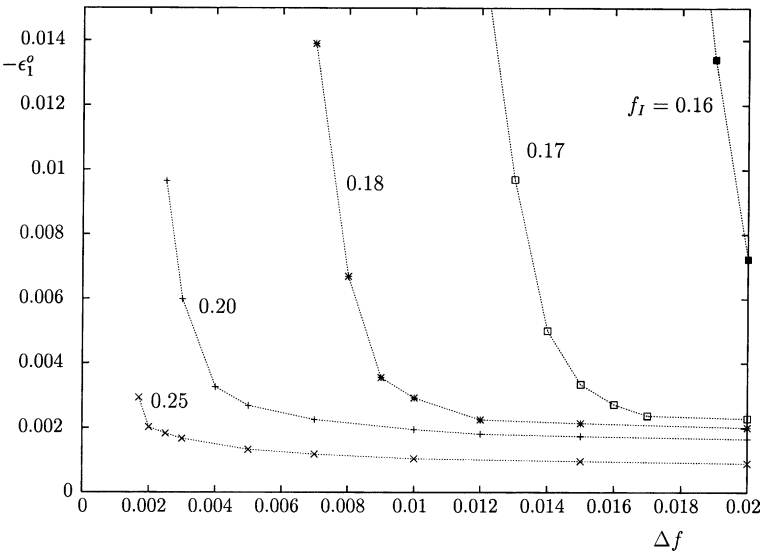

Fig. 3. Localization strain vs. initial porosity imperfection for plane strain conditions, $\epsilon_3^{\circ} = 0$, for different initial porosities with $\kappa = 0.10$, $n = 10$, and $\psi_I = 55°$.

duced rapidly for increasing Δf and all curves plateau at high imperfection amplitudes. At $f_I = 0.15$, no instability was found in the imperfection range studied due to the higher material cohesive strength.

Localization is found only when the material in the band undergoes dilatation, which corresponds to stress states on the parts of the yield surfaces in Fig. 1, where the normal to the yield surface has a positive component on the abscissa. In order to clarify this, the evolution of porosity inside and outside the band, f^{b} and f^{o}, during compaction are shown in Figs. 4 and 5, respectively. The curves represent three different initial porosities, $f_I = 0.15$, 0.16 and 0.18, with different localization behaviour. The porosity amplitude is $\Delta f = 0.02$ and the stress ratio is $\kappa = \sigma_2^{\mathrm{o}}/\sigma_1^{\mathrm{o}} = 0.10$, hence, the curves correspond to the far most right points in the previous figure. No localization occurs for $f_I = f^{\mathrm{o}} = 0.15$ as both f^{b} and f^{o} decrease with compaction. For the material with a slightly higher initial porosity, $f_I = 0.16$, the porosity inside the band increases slowly until the point of localization after which it increases rapidly. The stress ratio is kept fixed also after the onset of localization, hence, unloading of the material outside the band results in a sign change of the logarithmic strain rate. When the initial porosity is $f_I = 0.18$, localization does not occur in the usual sense, since plastic yielding never occurs outside the band, but the macroscopic material softening starts soon after the onset of yielding inside the band.

The same plane strain case is considered in Fig. 6 but for different levels of transverse compression while the initial porosity is kept fixed at $f_I = 0.25$. Here, the curve for $\kappa = \sigma_2^{\mathrm{o}}/\sigma_1^{\mathrm{o}} = 0.10$ is identical to that shown for $f_I = 0.25$ in Fig. 3. Shear bands are easily formed when the transverse stress is low, whereas rather high imperfection amplitudes are needed to obtain instabilities at higher transverse stresses. The critical strain increases with increased stress ratio. Higher values of κ were tested, e.g. $\kappa = 0.25$, but no localization was found as no dilation takes place even at large imperfections. At imperfection amplitudes higher than approximately $\Delta f = 0.01$ the strong dependence on the degree of transverse compression almost disappears for the four curves shown.

In Fig. 7, the degree of transverse stress is studied in a material with lower initial porosity, $f_I = 0.18$, but otherwise identical to the material considered in Fig. 6. Curves of the localization strain, $-\epsilon_1^{\mathrm{o}}$, vs. the initial porosity imperfection, Δf, for the low porosity material are shown. The result of $\kappa = 0.10$ was also seen in Fig. 3. The initial cohesive strength at $f_I = 0.18$ is $\eta \approx 0.15$, which is significantly higher than $\eta \approx 0.02$ at

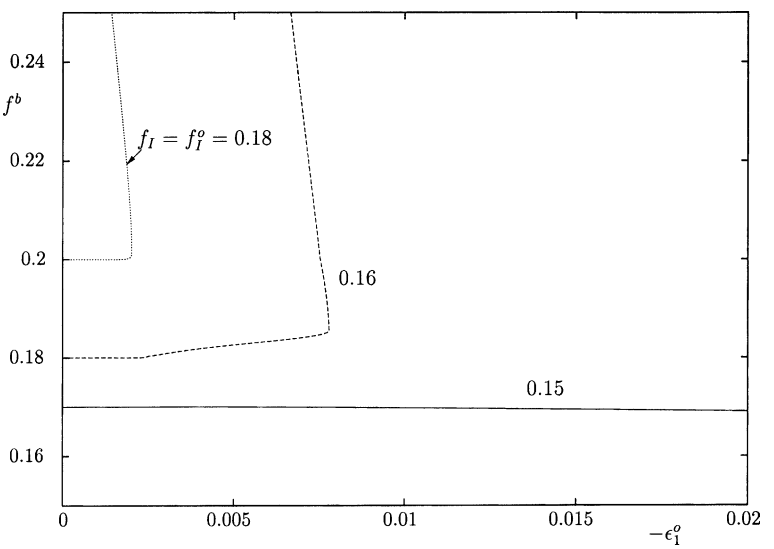

Fig. 4. Evolution of porosity in the band vs. logarithmic strain, $-\epsilon_1^{\mathrm{o}}$, for plane strain conditions, $\epsilon_3^{\mathrm{o}} = 0$, for different initial porosities with $\kappa = 0.10$, $n = 10$, and $\psi_I = 55°$.

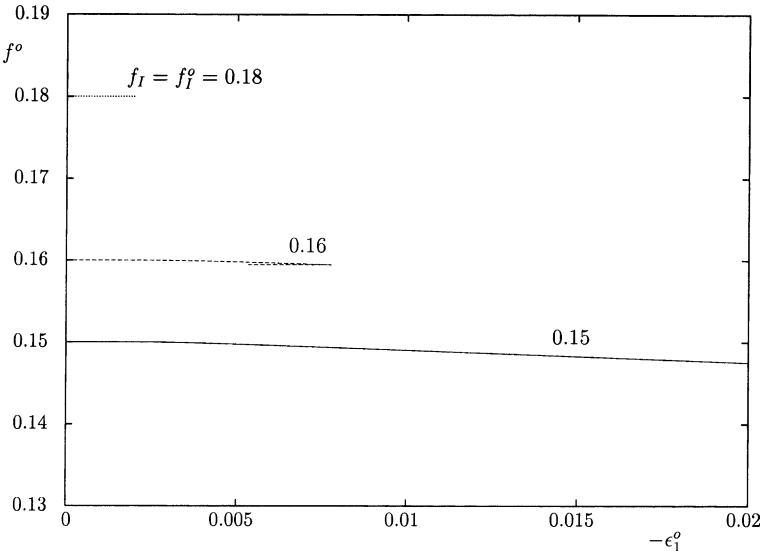

Fig. 5. Evolution of porosity outside the band vs. logarithmic strain, $-\epsilon_1^o$, for plane strain conditions, $\epsilon_3^o = 0$, for different initial porosities with $\kappa = 0.10$, $n = 10$, and $\psi_I = 55°$.

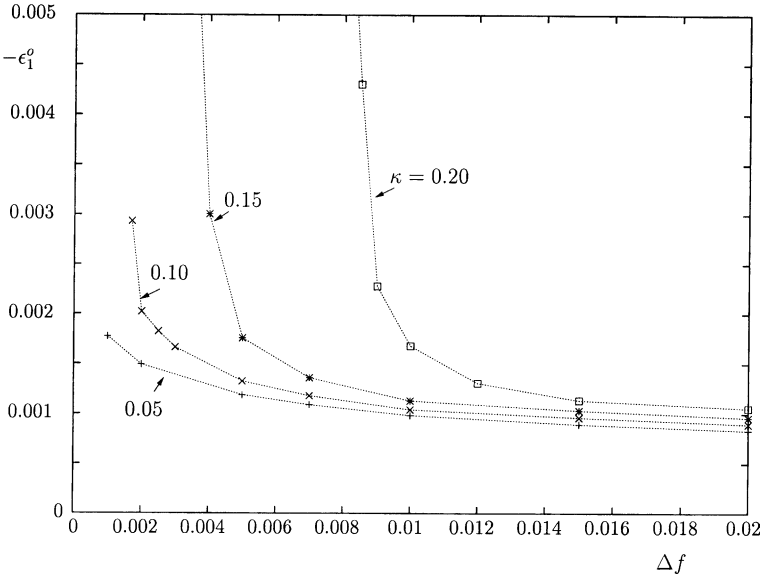

Fig. 6. Localization strain vs. initial porosity imperfection for plane strain conditions, $\epsilon_3^o = 0$, for different levels of transverse compression with $f_I = 0.25$, $n = 10$, and $\psi_I = 55°$.

$f_I = 0.25$ from the previous figure. The higher cohesive strength leads to later localization, and higher porosity imperfections are necessary to form the shear bands. Furthermore, the stress ratio $\kappa = \sigma_1^o/\sigma_2^o = 0.20$ does not lead to formation of shear bands in compression for this lower porosity ma-

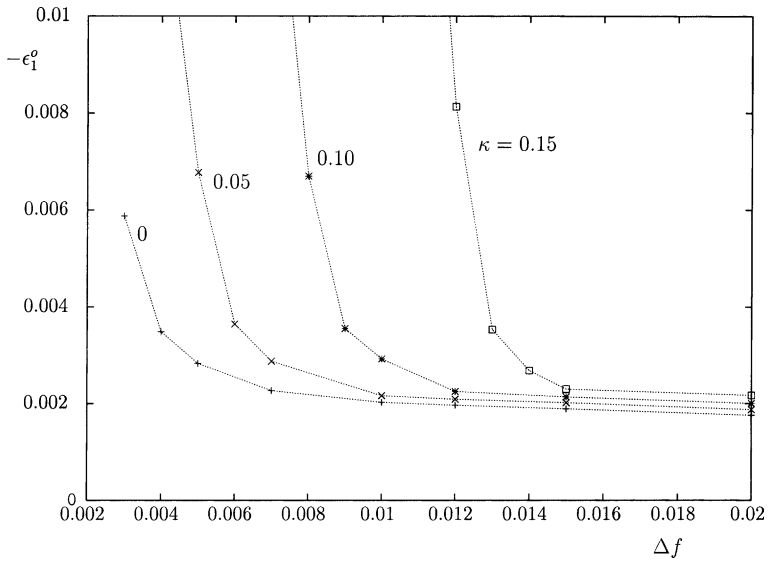

Fig. 7. Localization strain vs. initial porosity imperfection for plane strain conditions, $\epsilon_3^o = 0$, for different levels of transverse compression with $f_I = 0.18$, $n = 10$, and $\psi_I = 55°$.

terial, whereas instabilities are observed at the higher porosity for the same degree of transverse stress (see Fig. 6).

The dependence on the initial angle of inclination, ψ_I, is shown in Fig. 8 for a material with $f_I = 0.18$ and $\Delta f = 0.008$ under plane strain conditions. Different levels of transverse compression are shown. As expected, there is a strong sensitivity to the initial band orientation, such that the lowest critical strain occurs at a value around 53° for $\kappa = 0.10$ and down to about 50° for lower values of transverse stresses. At

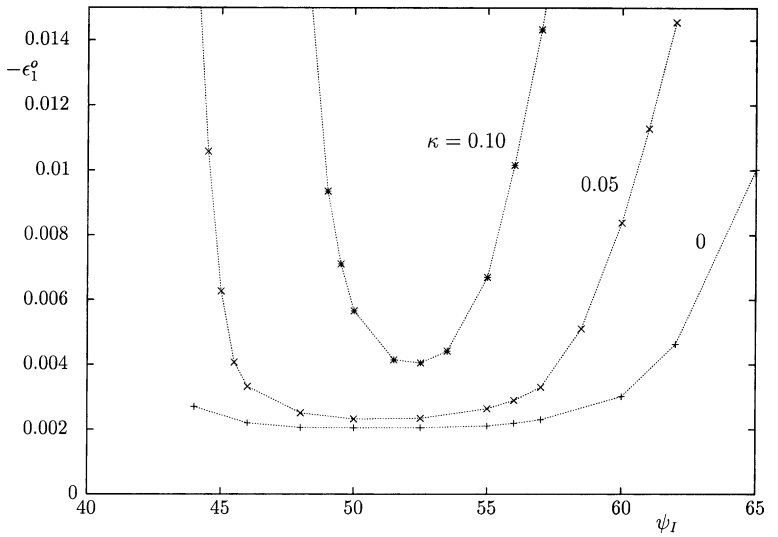

Fig. 8. Localization strain vs. initial band orientation for plane strain conditions, $\epsilon_3^o = 0$, for different levels of transverse compression with $f_I = 0.18$, $\Delta f = 0.008$ and $n = 10$.

uniaxial plane strain compression, $\kappa = 0$, the critical strain values are almost constant in a wide range of ψ_I values. In fact, the strain values shown on the flat part of the curve, $47° < \psi_I < 53°$, are not localizations in the usual sense, since the material outside the band never yields, and the strain shown is the maximum value reached outside the band, which occurs slightly after the onset of yielding inside the band. A similar localization behaviour was shown in Figs. 4 and 5. A slight increase in the transverse stress, $\kappa = 0.05$, results in true localization strains in the whole range of inclination angles considered.

Fig. 9 illustrates the effect of stress triaxiality under axisymmetric conditions, $\epsilon_3^o = \epsilon_2^o$, outside the band. The set of material parameters considered are the same as in Fig. 8, but with the porosity imperfection set to a rather high value, $\Delta f = 0.03$. Even at this high initial imperfection, the localization strains are quite high compared to the plane strain results in Fig. 8 showing plane strain conditions with a much smaller porosity imperfection, $\Delta f = 0.008$. That localization strains are significantly higher for axisymmetric conditions has been shown earlier, e.g. for the Gurson model in tension (see Redanz and Tvergaard, 1999). Again, there is no true localization at the flat parts of the curves, as no yielding outside the band takes place. However, the critical strains pick up at $\psi_I \geqslant 60°$ and increase significantly with increased inclination angle even at uniaxial compression, $\kappa = 0$. At $\kappa = 0.20$, all points shown represent true localization, whereas no shear bands are formed at the higher stress triaxiality, $\kappa = 0.25$.

The dependence on the imperfection amplitude is shown for axisymmetric conditions at different levels of stress triaxialities in Fig. 10. The inclination angle is $\psi_I = 65°$, hence, the results for $\Delta f = 0.03$ correspond to the 65° data points shown in Fig. 9. In Fig. 10, the critical strain curves do not increase rapidly at lower porosity imperfections, as in the plane strain case, instead the curves show a point of inflection as Δf decays.

We have no direct experimental comparison for shear band formation in metal powder compaction. However, it is noted that in both plane strain and triaxial compression tests of e.g. dense sand and stiff merl the localization strain varies from about −0.04 to −0.004 and even lower for loose sand (see e.g. Oda and Kazama, 1998; Desrues and Chambon, 2002). These localization strains are of the same order of magnitude as those found in the present analyses.

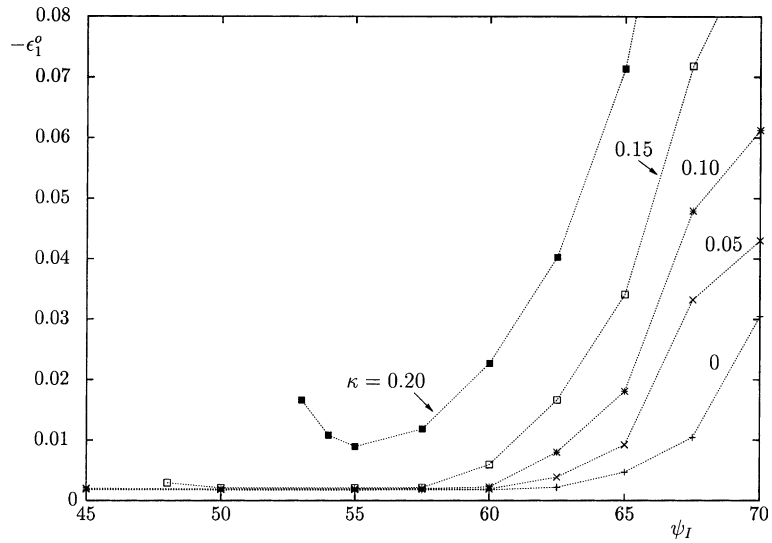

Fig. 9. Localization strain vs. initial band orientation for axisymmetric conditions, $\epsilon_3^o = \epsilon_2^o$, for different levels of transverse compression with $f_I = 0.18$, $\Delta f = 0.03$ and $n = 10$.

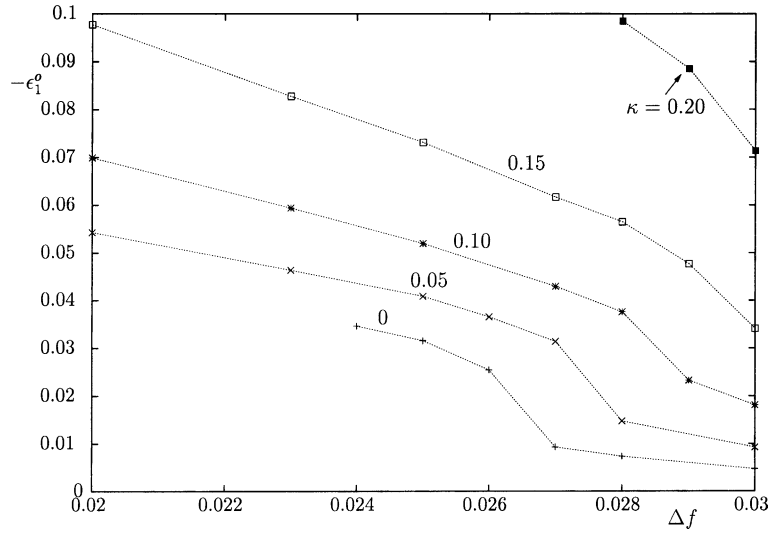

Fig. 10. Localization strain vs. initial porosity imperfection for axisymmetric conditions, $\epsilon_3^o = \epsilon_2^o$, for different levels of transverse compression with $f_I = 0.18$, $n = 10$, and $\psi_I = 65°$.

5. Discussion

For the metal powder compaction process the material model proposed by Fleck et al. (1992) appears to be very reasonable, using an interpolation between two micro-mechanically based models, the FKM model appropriate for high porosity levels with particles connected by isolated necks, and the Gurson model appropriate for much lower porosity levels, with the porosity present in the form of isolated voids. In this case the interpolation with the Gurson model is necessary, since the FKM model is not applicable at low porosities, i.e. $f < 0.10$. However, the fact that this model does not predict any localization of plastic flow in shear bands under compressive loading (Redanz and Tvergaard, 1999) illustrates that something is missing. When using the modified version of the FKM model proposed by Fleck (1995), which introduces a cohesion factor to be able to represent a low level of inter-particle cohesion, it has been shown (Tvergaard and Redanz, 2001) that shear localization under compressive loading is predicted in some cases.

Based on these results, a more realistic material model for metal powder compaction is proposed in the present paper. This model is based on an interpolation between the low inter-particle cohesion model proposed by Fleck (1995) and the Gurson model. The model also introduces a linear variation of the cohesion factor with the porosity level. For high porosity levels this model predicts shear band instabilities, as would be expected since the model is practically identical to that of Fleck (1995) in this range. The low inter-particle cohesive strength in the highly porous material makes it possible to obtain stress states in compression leading to dilatation and thereby possibly shear band instabilities. Also in an intermediate range of porosities it has been shown here that shear localization can still occur, if the stress triaxiality is not too large. However, for the parameter values chosen in the present analyses no localization is predicted under compressive loading if the level of porosity is quite low.

It is noted that if the Gurson model is not involved at all in the material model proposed here, so that the only dependence on the porosity f is that involved in the proposed linear dependence of the cohesion factor on f, in addition to the dependence already included in the model proposed by Fleck (1995), the model would not be realistic at small porosities. Even for a small value of the cohesion factor η the model would allow for unrealistic yield stresses larger than that of the fully dense material if $f < 0.10$. Using the Gurson

model in the range of small porosities is considered realistic for compressive stresses but for tensile stresses the model will overestimate the strength of the green specimen.

Acknowledgements

The work was partly supported by the FREJA research project, Application of Advanced Material Models in the Analysis of Metal Forming Processes, financed by the Danish Research Agency.

References

Arzt, E., 1982. The influence of an increasing particle co-ordination on the densification of spherical powders. Acta Metall. 30, 1883–1890.

Arzt, E., Ashby, M.F., Easterling, K.E., 1983. Metall. Trans. 14A, 211.

Desrues, J., Chambon, R., 2002. Shear band analysis and shear moduli calibration. Int. J. Solids Struct. 39, 3757–3776.

Fleck, N.A., 1995. On the cold compaction of powders. J. Mech. Phys. Solids 43, 1409–1431.

Fleck, N.A., Kuhn, L.T., McMeeking, R.M., 1992. Yielding of metal powder bonded by isolated contacts. J. Mech. Phys. Solids 40 (5), 1139–1162.

Gurson, A.L., 1977. Continuum theory of ductile rupture by void nucleation and growth— I. Yield criteria and flow rules for porous ductile media. J. Engng. Mater. Technol. 99, 2–15.

Helle, A.A., Easterling, K.E., Ashby, M.F., 1985. Hot-isostatic pressing diagrams: new developments. Acta Metall. 33 (12), 2163–2174.

Lade, P.V., 1977. Elastic–plastic stress–strain theory for cohesionless soil with curved yield surfaces. Int. J. Solids Struct. 13, 1019–1035.

Oda, M., Kazama, H., 1998. Microstructure of shear bands and its relation to the mechanisms of dilatancy and failure of dense granular soils. Geotechnique 48, 465–481.

Redanz, P., 1999. Numerical modelling of the powder compaction of a cup. Eur. J. Mech. A/Solids 18, 399–413.

Redanz, P., 2001. A study of stresses in powder compacted components during and after ejection. Int. J. Solids Struct. 38 (5), 759–775.

Redanz, P., Tvergaard, V., 1999. Analysis of shear band instabilities in sintered metals. Int. J. Solids Struct. 36, 3661–3676.

Rice, J., 1976. The localization of plastic deformation. In: Koiter, W.T. (Ed.), Proc. 14th Int. Congr. Theor. Appl. Mech. North-Holland, Amsterdam, pp. 207–220.

Rudnicki, J.W., Rice, J.R., 1975. Conditions for the localization of deformation in pressure-sensitive dilatant materials. J. Mech. Phys. Solids 23, 371–394.

Saje, M., Pan, J., Needleman, A., 1982. Void nucleation effects on shear localization in porous plastic solids. Int. J. Fract. 19, 163–182.

Schofield, A., Wroth, C.P., 1968. Critical State Soil Mechanics. McGraw-Hill.

Tvergaard, V., 1981. Influence of voids on shear band instabilities under plane strain conditions. Int. J. Fract. 17, 389–407.

Tvergaard, V., 1982a. On localization in ductile materials containing spherical voids. Int. J. Fract. 18, 237–252.

Tvergaard, V., 1982b. Material failure by void coalescence in localized shear bands. Int. J. Solids Struct. 18, 659–672.

Tvergaard, V., 1990. Material failure by void growth to coalescence. Adv. Appl. Mech. 27, 83–151.

Tvergaard, V., Redanz, P., 2001. Shear band instabilities in compacted metal powder with or without interparticle cohesion. J. Phys. IV 11, 339–347.

Yamamoto, H., 1978. Conditions for shear localization in the ductile fracture of void-containing materials. Int. J. Fract. 14, 347–365.